AGU PUBLICATIONS

Tectonics

RESEARCH ARTICLE

10.1002/2014TC003695

Key Points:
- The plate boundary fault at the Japan Trench is described from drill core
- Sharp faults cut distributed scaly fabric in clay-rich fault rock
- Structures record velocity-dependent stability and past slip to the trench

Correspondence to:
J. D. Kirkpatrick,
james.kirkpatrick@colostate.edu

Citation:
Kirkpatrick, J. D., et al. (2015), Structure and lithology of the Japan Trench subduction plate boundary fault, *Tectonics*, *34*, 53–69, doi:10.1002/2014TC003695.

Received 27 JUL 2014
Accepted 6 DEC 2014
Accepted article online 12 DEC 2014
Published online 21 JAN 2015

Structure and lithology of the Japan Trench subduction plate boundary fault

James D. Kirkpatrick[1], Christie D. Rowe[2], Kohtaro Ujiie[3], J. Casey Moore[4], Christine Regalla[5], Francesca Remitti[6], Virginia Toy[7], Monica Wolfson-Schwehr[8], Jun Kameda[9], Santanu Bose[10], and Frederick M. Chester[11]

[1]Department of Geosciences, Colorado State University, Fort Collins, Colorado, USA, [2]Department of Earth and Planetary Sciences, McGill University, Montréal, Québec, Canada, [3]Graduate School of Life and Environmental Sciences, University of Tsukuba, Tsukuba, Japan, [4]Department of Earth and Planetary Sciences, University of California, Santa Cruz, California, USA, [5]Department of Geosciences, Pennsylvania State University, University Park, Pennsylvania, USA, [6]Dipartimento di Scienze Chimiche e Geologiche, Università di Modena e Reggio Emilia, Modena, Italy, [7]Department of Geology, University of Otago, Dunedin, New Zealand, [8]Center for Coastal and Ocean Mapping, Joint Hydrographic Center, University of New Hampshire, Durham, New Hampshire, USA, [9]Department of Natural History Sciences, Faculty of Science, Hokkaido University, Sapporo, Japan, [10]Department of Geology, University of Calcutta, Kolkata, India, [11]Center for Tectonophysics, Department of Geology and Geophysics, Texas A&M University, College Station, Texas, USA

Abstract The 2011 M_w9.0 Tohoku-oki earthquake ruptured to the trench with maximum coseismic slip located on the shallow portion of the plate boundary fault. To investigate the conditions and physical processes that promoted slip to the trench, Integrated Ocean Drilling Program Expedition 343/343T sailed 1 year after the earthquake and drilled into the plate boundary ~7 km landward of the trench, in the region of maximum slip. Core analyses show that the plate boundary décollement is localized onto an interval of smectite-rich, pelagic clay. Subsidiary structures are present in both the upper and lower plates, which define a fault zone ~5–15 m thick. Fault rocks recovered from within the clay-rich interval contain a pervasive scaly fabric defined by anastomosing, polished, and lineated surfaces with two predominant orientations. The scaly fabric is crosscut in several places by discrete contacts across which the scaly fabric is truncated and rotated, or different rocks are juxtaposed. These contacts are inferred to be faults. The plate boundary décollement therefore contains structures resulting from both distributed and localized deformation. We infer that the formation of both of these types of structures is controlled by the frictional properties of the clay: the distributed scaly fabric formed at low strain rates associated with velocity-strengthening frictional behavior, and the localized faults formed at high strain rates characterized by velocity-weakening behavior. The presence of multiple discrete faults resulting from seismic slip within the décollement suggests that rupture to the trench may be characteristic of this margin.

1. Introduction

The devastating 2011 M_w9 Tohoku-oki earthquake ruptured a 200 x 380 km area of the Japan Trench plate boundary where the Pacific Plate subducts beneath Japan. Coseismic slip associated with the event was the largest ever recorded, reaching >50 m in teleseismic, GPS, and tsunami slip models [*Fujii et al.*, 2011; *Ide et al.*, 2011; *Lay et al.*, 2011; *Pollitz et al.*, 2011; *Yue and Lay*, 2011]. Observations of seafloor movement also imply large slip and show that the earthquake ruptured to the trench [*Fujiwara et al.*, 2011; *Ito et al.*, 2011; *Kodaira et al.*, 2012]. Slip which increased toward the trench is exceptional for subduction zone megathrust earthquakes that typically display maximum slip within the seismogenic zone. Large, shallow slip directly contributed to the generation of the tsunami that inundated the coastal areas of Honshu and propagated around the Pacific Ocean.

Integrated Ocean Drilling Program (IODP) Expedition 343, the "Japan Trench Fast Earthquake Drilling Project (JFAST)", sailed 1 year after the earthquake to investigate the conditions and physical processes that facilitated large slip at shallow depth [*Chester et al.*, 2013a]. The plate boundary was drilled in water depths of nearly 7000 m at Site C0019, within the area of highest coseismic displacement of the Tohoku-oki earthquake (Figure 1). Multiple results from the expedition point to a weak plate boundary fault, both coseismically and over geologic time scales. Measurements of the anisotropy of magnetic susceptibility from core samples show a distinct change in orientation across the plate boundary suggesting decoupling

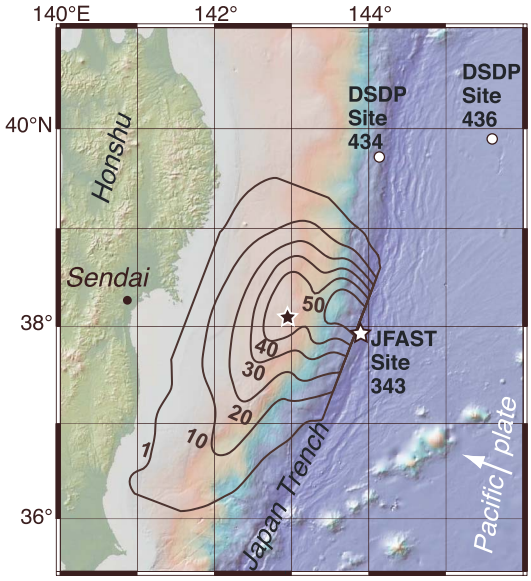

Figure 1. Location of the JFAST study site (IODP Expedition 343 Site C0019). Map shows the coast of Honshu and the extent of the 2011 Tohoku-oki earthquake rupture. Contours of slip during the 2011 Tohoku-oki rupture are taken from *Yue and Lay* [2011]; slip amount in meters is labeled. White arrow shows the convergence direction between the Pacific Plate and the Japan Trench.

between the upper and lower plates and implying that the plate boundary fault is weak over geologic time [*Yang et al.*, 2013]. Borehole breakout analyses show that the stress field in the frontal prism is currently in a normal faulting stress regime, suggesting a large coseismic stress drop [*Lin et al.*, 2013]. Measurements of the temperature in and around the plate boundary fault in the postseismic period show that the shear resistance to slip on the shallow portion of the rupture was 0.53 MPa [*Fulton et al.*, 2013], consistent with expectations from rock friction experiments [*Faulkner et al.*, 2011; *Ujiie et al.*, 2013]. These observations, in combination with seismological observations of numerous normal faulting aftershocks in the upper plate [*Hasegawa et al.*, 2012], indicate minimal resistance to shear during the 2011 Tohoku-oki earthquake and nearly complete decoupling of the plate boundary.

Rupture propagation and slip are controlled, in part, by the internal structure of the fault, which in turn is the product of the accumulated deformation and alteration. One of the key physical parameters is the composition of the fault rocks, which influences the strength and frictional stability, the degree of shear localization during slip, and the likely slip weakening mechanisms active during an earthquake [e.g., *Marone*, 1998; *Rice and Cocco*, 2007; *Ikari et al.*, 2011; *Niemeijer et al.*, 2012]. Geophysical logs and structural observations of the C0019E drill core collected during the JFAST project show that the plate boundary is localized onto a relatively thin layer of pelagic clay [*Chester et al.*, 2013b]. The pelagic clay is smectite-rich [*Ujiie et al.*, 2013; *Kameda et al.*, 2015; A. M. Schleicher et al., Response of natural smectite to seismogenic heating and implications for the 2011 Tohoku earthquake in the Japan Trench, submitted to *Geology*, 2014], and rock friction experiments on samples of the core show that the clay is frictionally weak, velocity-weakening at seismic slip rates [*Ujiie et al.*, 2013], and is weaker than the surrounding mudstones [*Ikari et al.*, 2015]. This combination of properties suggests that localization of slip onto the thin plate boundary fault is preferred during both seismic and aseismic deformation during the seismic cycle [*Chester et al.*, 2013b].

Here we present an overview of the observations of core from the JFAST study site to identify the materials and structures that control the mechanical behavior of the shallow part of the subduction megathrust, expanding upon the observations of *Chester et al.* [2013a, 2013b]. Approximately 55 m of discontinuous core from hole C0019E were recovered during Expedition 343 that sampled the frontal prism, décollement, and down-going Pacific Plate [*Chester et al.*, 2013b]. Unlike other forearcs, whose frontal prism structure is clearly imaged in seismic data (e.g., Sumatra, Nankai), the frontal prism at the Japan Trench is acoustically chaotic [*Chester et al.*, 2013a; *Nakamura et al.*, 2013]. Although the décollement is marked by a continuous seismic reflector [e.g., *Nakamura et al.*, 2013], the lack of seismically resolvable structures within the frontal prism means that the plate boundary architecture is best studied from core observations and geophysical logs.

In the following sections we review the observations that define the contacts at the base of the frontal prism and the top of the Pacific Plate sedimentary rocks to define the location and thickness of the plate boundary fault. The total displacement of the footwall relative to the hanging wall at the study site is estimated to be around 3.2 km, based on an area-balanced reconstruction of a seismic section through the study site in the plate convergence direction [*Chester et al.*, 2013b]. We incorporate structural and sedimentological observations of the core and radiolarian biostratigraphic ages to document the structures surrounding the previously identified décollement. These observations, along with details of the deformation fabrics within the décollement fault rocks, are used to infer the relative strain rates of formation and to develop an interpretation of the mechanical behavior of the shallow part of the décollement.

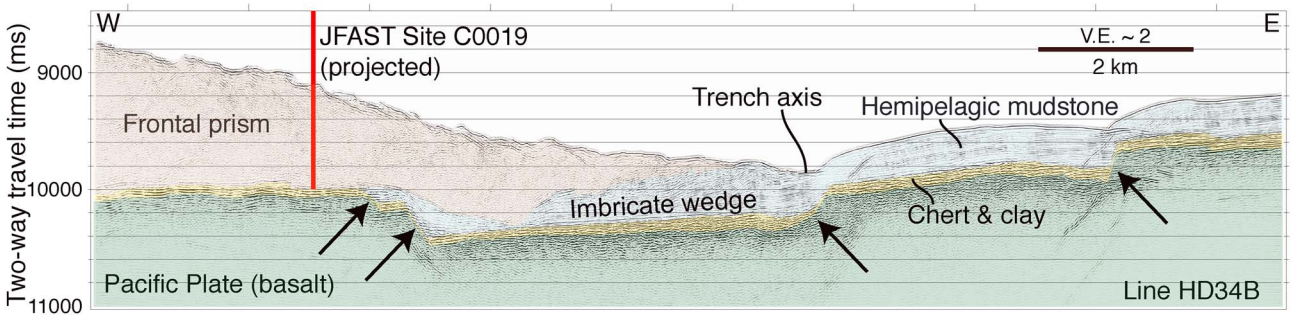

Figure 2. Seismic section perpendicular to the Japan Trench located ~500 m north of the JFAST study site showing the tectonic setting and overall structure of the margin (adapted from *Nakamura et al.* [2013]). Locations of normal faults are shown with arrows, and the colors correspond to the different seismic units identified by *Nakamura et al.* [2013].

2. Tectonic Setting

The JFAST study site (IODP Site C0019) was located approximately 250 km off the Pacific coast of Sendai, Japan, and 100 km ESE of the epicenter of the 2011 Tohoku-oki earthquake (Figure 1). The site is 7 km landward of the Japan Trench, where the Pacific Plate subducts beneath Japan at a convergence rate of 85 mm/yr [*DeMets et al.*, 2010; *Argus et al.*, 2011]. This rapid convergence results in a high rate of seismic activity. The historical record for the region includes 13 *M*7 and five *M*8 earthquakes over the last 400 years, in addition to the 2011 M_w9 event and its aftershock sequence [e.g., *Hashimoto et al.*, 2009; *Kanamori et al.*, 2006].

The margin is characterized by an ~8 km deep trench with a shallowly dipping (~8°) décollement [*von Huene et al.*, 1982]. Seismic reflection surveys [*von Huene et al.*, 1982; *Tsuru et al.*, 2002, 2005; *Kodaira et al.*, 2012; *Nakamura et al.*, 2013] combined with previous drilling expedition results [*Arthur and Adelseck*, 1980] and the results of the JFAST expedition [*Chester et al.*, 2013b; *Nakamura et al.*, 2013] show that the incoming Pacific Plate is composed of a basement of basaltic rocks overlain by a seismically resolvable unit of chert and a sequence of pelagic clay and hemipelagic mudstone (Figure 2). Both the basement and the entire sedimentary section are cut by normal faults. By analogy with active faults at the outer rise, we infer that the horst-and-graben topography developed within 50–100 km of the trench.

The seaward ~6 km of the prism toe at Site C0019 structurally overlies a graben in the oceanic crust (Figure 2). Within this graben, the hemipelagic sediments are imbricated along listric thrust faults spaced a few hundred meters apart that sole into the proto-plate boundary décollement. This small imbricate wedge transitions landward to a thicker, acoustically chaotic wedge that comprises most of the frontal prism [*Nakamura et al.*, 2013]. The JFAST drill site is located above the frontal prism where it overlies a subducted horst.

3. The Frontal Prism and Pacific Plate

Approximately 55 m of discontinuous core was recovered in 21 coring runs from IODP hole C0019E [*Chester et al.*, 2013a]. Operational constraints required targeted recovery from specific intervals separated by advances with no core recovery: core 1R was recovered from ~175–185 m below sea floor (mbsf); cores 2R and 3R from ~648–660 mbsf; cores 4R through 9R from ~690–725 mbsf; and cores 10R to 21R from ~770–835 mbsf. All cores required splitting with a rock saw indicating the prism is lithified throughout the sampled depth ranges, consistent with observations along strike at Deep Sea Drilling Project (DSDP) sites 441 and 434 [*Carson et al.*, 1982]. Recovery was incomplete in each core (Figure 3), meaning that even within the targeted intervals, the core is discontinuous. In this section, we briefly review observations from *Chester et al.* [2013a] of the lower part of the prism and the sedimentary rocks of the Pacific Plate below to establish the location of the décollement and the nature of the surrounding structures.

3.1. Frontal Prism

The majority of cores recovered from the prism (2R to 16R) contain olive-gray to very dark gray and grayish brown hemipelagic mudstones. Overall, these mudstones contain dominant silicilastic clay-sized and silt-sized grains, typically with a few to 15% siliceous microfossils. They are interbedded with intermittent

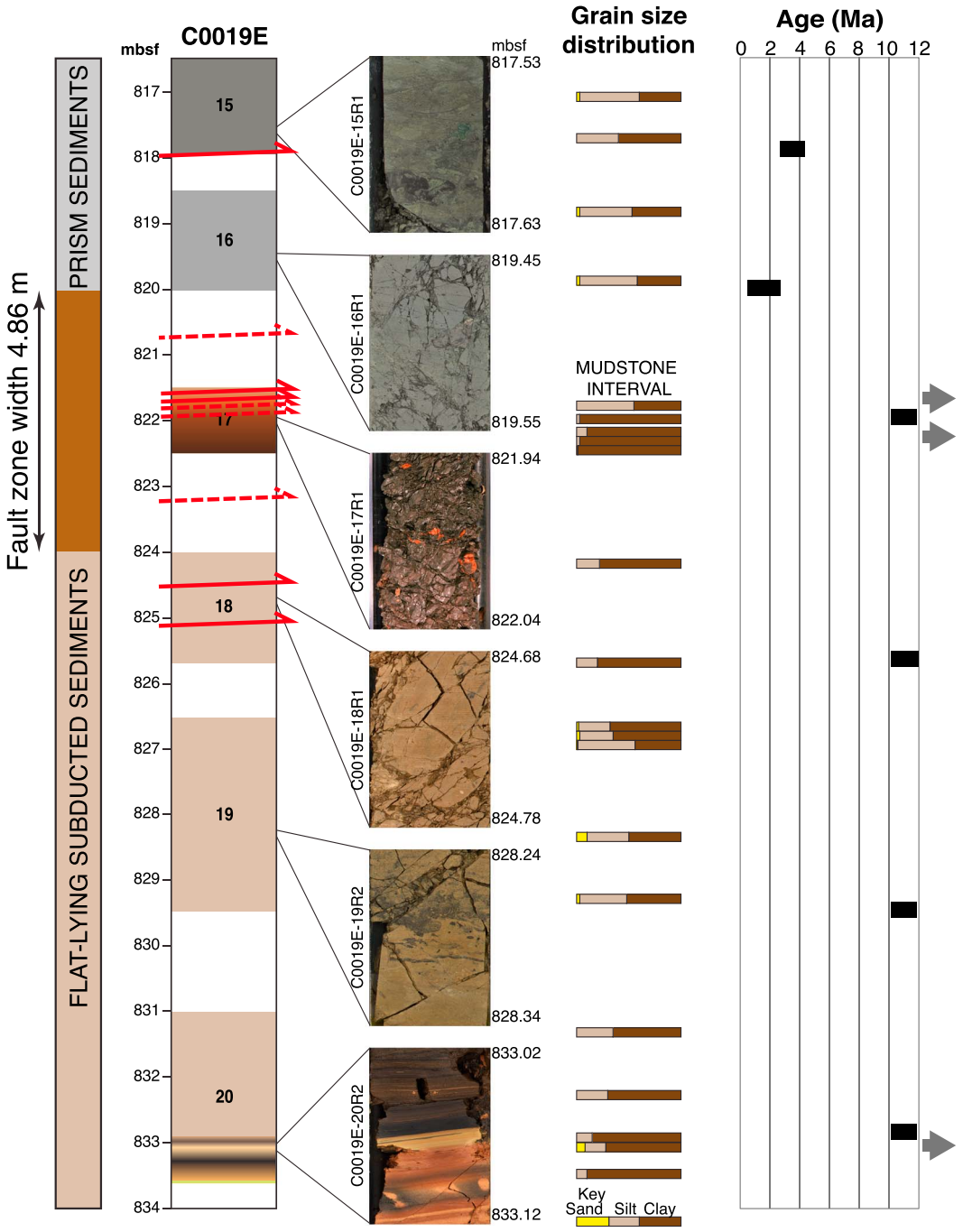

Figure 3. Context of the plate boundary décollement in core C0019C. Core recovery and lithology are shown in the column headed C0019E; white gaps represent nonrecovered intervals. Representative photos from each of the recovered cores showing the characteristic lithology and structures, the grain size distribution based on qualitative smear slide analysis, and the biostratigraphic age of the rocks are shown from left to right at depths corresponding to the depth scale on the left (based on information from *Chester et al.* [2013a]). Grey arrows at the right of the age plot indicate that the rocks are older than Miocene. The fault zone width shown on the left-hand side of the figure is based on drilling logs recording the advance of the bit from the base of the frontal prism to the top of the Pacific Plate [*Chester et al.*, 2013b]. Note that bit advance and curated core lengths differ due to core processing. Red arrows indicate the locations of observed faults and dashed red arrows represent faults inferred from stratigraphic age reversals and gaps.

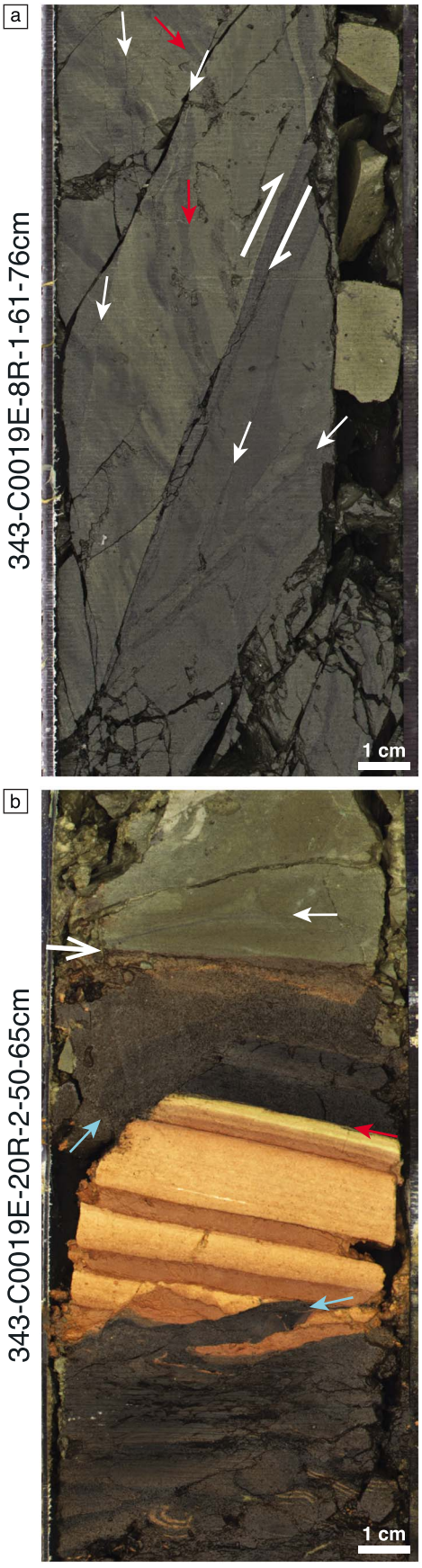

centimeter-scale clay or silt beds and range from locally ashy to volcaniclastic poor. Biostratigraphic ages determined from microfossil assemblages show that the rocks are Pleistocene to Miocene in age [*Chester et al.*, 2013a], but the units are both repeated and out of sequence, indicating tectonic interleaving (Figure 3).

Bedding orientations are generally moderately to steeply dipping (~20–80°) and are rarely overturned, and poles to bedding define a π-girdle consistent with folding and thrusting accommodating shortening in the plate convergence direction [*Chester et al.*, 2013a]. The frequency of the biostratigraphic age reversals and gaps, along with the bedding orientations, indicate that the frontal prism units are imbricated by numerous thrusts. Closely spaced faults are consistent with the poorly resolved, semicontinuous landward dipping reflectors within generally acoustically chaotic seismic images through prism beneath the JFAST site [*Nakamura et al.*, 2013].

Several faults with displacements greater than the diameter of the core (~6 cm) and numerous core-scale structures are visible cores 2R to 16R. Core-scale structures include centimeter-offset shear fractures with both normal and reverse offsets, anastomosing dark seams of fault rock (similar to structures described by *Ujiie et al.* [2004]) and sediment-filled veins. Faults are defined predominantly from bedding cutoffs and typically contain several millimeters to several centimeters of fine-grained, generally dark gray to black fault rock. The faults are moderately to steeply dipping, but none of the core-scale faults juxtaposed different lithologies. Bedding dips

Figure 4. (a) Multiscanner core logger image (MSCL-I) of the fault at 720 mbsf (note that the format of the image labels on the left is as follows: expedition-hole-core-section-distance from section top (range in centimeters), following standard IODP convention). The fault is defined by hanging wall bedding cutoffs against a sharp contact (bedding shown by red arrows). Large white arrows in the center of the image show the inferred sense of shear across the contact. Smaller white arrows are examples of core-scale structures developed in and around the fault. (b) MSCL-I image of the contact at the base of the Miocene mudstone where it overlies Cretaceous laminar clay (832.85 mbsf). Large white arrow points to the pinkish layer present at the contact, red arrow shows the bedding attitude. Only one dark seam is present structurally above the contact (small white arrow). Small cyan arrows show places where clay laminations are not visible, probably because of drilling-induced disturbance.

that steepen toward one fault at 720 mbsf are consistent with drag folding or fault propagation folding around a reverse fault (Figure 4). One example of a fault near the base of core 15R contains a dense array of millimeter-thick seams of fault rock inferred to be shear fractures from the lack of continuity in the mudstone sedimentary fabrics. The density of shear fractures increases down-core to a ~10 cm thick layer of fault breccia and gouge containing clasts of the greenish gray mudstone wall rock.

3.2. Pacific Plate

Sedimentary rocks recovered from the deepest portions of the borehole (cores 18R to 21R) are mostly tan-brown terrigenous mudstones, which overly pelagic clay. A short interval of chert was recovered from the base of the hole. The mudstones are composed predominantly of siliciclastic grains, with a minor volcaniclastic component and trace siliceous microfossils. Smear slide grain size fraction estimates (Figure 3) show that siliciclastic grains are predominantly clayey (>60% clay) in the upper portion of the unit and become progressively siltier down-section (reaching >40% silt). Bedding in the tan-brown mudstone is indistinct, likely due to extensive bioturbation (indicated by mottling), but is marked by decimeter-scale fining-upward sequences in the lower part of the unit. Elsewhere, color variations from yellowish to grayish tan-brown occur across boundaries locally parallel to clay-rich, centimeter-scale interbeds. Subcentimeter sized, white pumice fragments are present throughout the unit.

Biostratigraphic ages show that the Miocene tan mudstone overlies a Cretaceous laminar pelagic clay [*Chester et al.*, 2013a] (Figure 3). The clay consists of a 50 cm thick interval of pinkish brown, creamy yellow and dark brown centimeter-scale interbeds of clay with millimeter-scale laminations. The contact between the clay and overlying Miocene mudstone is sharp and is marked by a ~1–3 mm thick pinkish, clayey layer at the base of the mudstone (at 832.85 mbsf; Figure 4). Bedding is difficult to identify in the mudstone immediately above the contact because the unit is bioturbated, but the few available attitude measurements based on the boundaries of bioturbated horizons suggest that the mudstone dips ~10–20°. Bedding is planar and subparallel in the pelagic clay, and beds dip 3–9°. Within the clay, the clay laminae are absent in irregular shaped zones (blue arrows in Figure 4b). These zones are interpreted to have formed due to biscuiting during drilling due to their irregular shapes. Very few deformation structures, with consistently small offsets (millimeter scale), are present in either the mudstone or clay around the contact. At the base of the clay, the unit becomes progressively greener and harder, due to silicification. The contact to silicified material is gradational and irregular, with isolated greenish yellow patches within the lower portion of the clay and 0.5 mm silica spherules becoming more common toward the base. Laminations similar to those in the clay are present within the silicified unit. The gradational contact at the base of the pelagic clay suggests that the transition to chert is a diagenetic silicification front rather than a stratigraphic or tectonic contact.

Based on the grain size distribution, volcaniclastic content and microfossil assemblages, the tan-brown mudstone in cores 18R–20R at the JFAST site correlates to Unit 2 at the nearest incoming plate reference site, DSDP Site 436 (for a detailed discussion of the stratigraphic correlation between Site C0019 and DSDP Site 436, see *Nakamura et al.* [2013] and *Moore et al.* [2015]). The Cretaceous pelagic clay and chert in cores 20R–21R at the JFAST site correlate with Cretaceous chert (Unit 3) at the DSDP reference site.

Two prominent faults cut the mudstone at 824.4 mbsf and 825.1 mbsf. Both of these faults are defined by a few centimeters thick layer that dips ~25–35° and cuts bedding. Within each fault layer, the rock is pinkish brown, relatively homogenous mudstone in which the primary sedimentary features are obliterated. Both faults have tan-brown mudstone on either side, implying that the fault displacement is less than the thickness of the mudstone. The maximum stratigraphic thickness of the mudstone is ~10.5 m, so for faults dipping 35° the maximum displacement is less than ~18 m. In addition to the two prominent faults, core-scale structures cutting the mudstone and clay include very narrow aperture, anastomosing fractures defining a fracture cleavage, shear fractures, dark seams, and open fractures. These structures are shallowly to steeply dipping and display both reverse and normal offsets.

4. The Décollement

4.1. Plate Boundary Location and Thickness

The transition from frontal prism to down-going plate sediments is marked by excursions in gamma ray intensity and resistivity values measured with logging-while-drilling (LWD) tools and a change in bedding orientations measured in resistivity images and in the core. It occurs at around 821.5 mbsf, the depth of

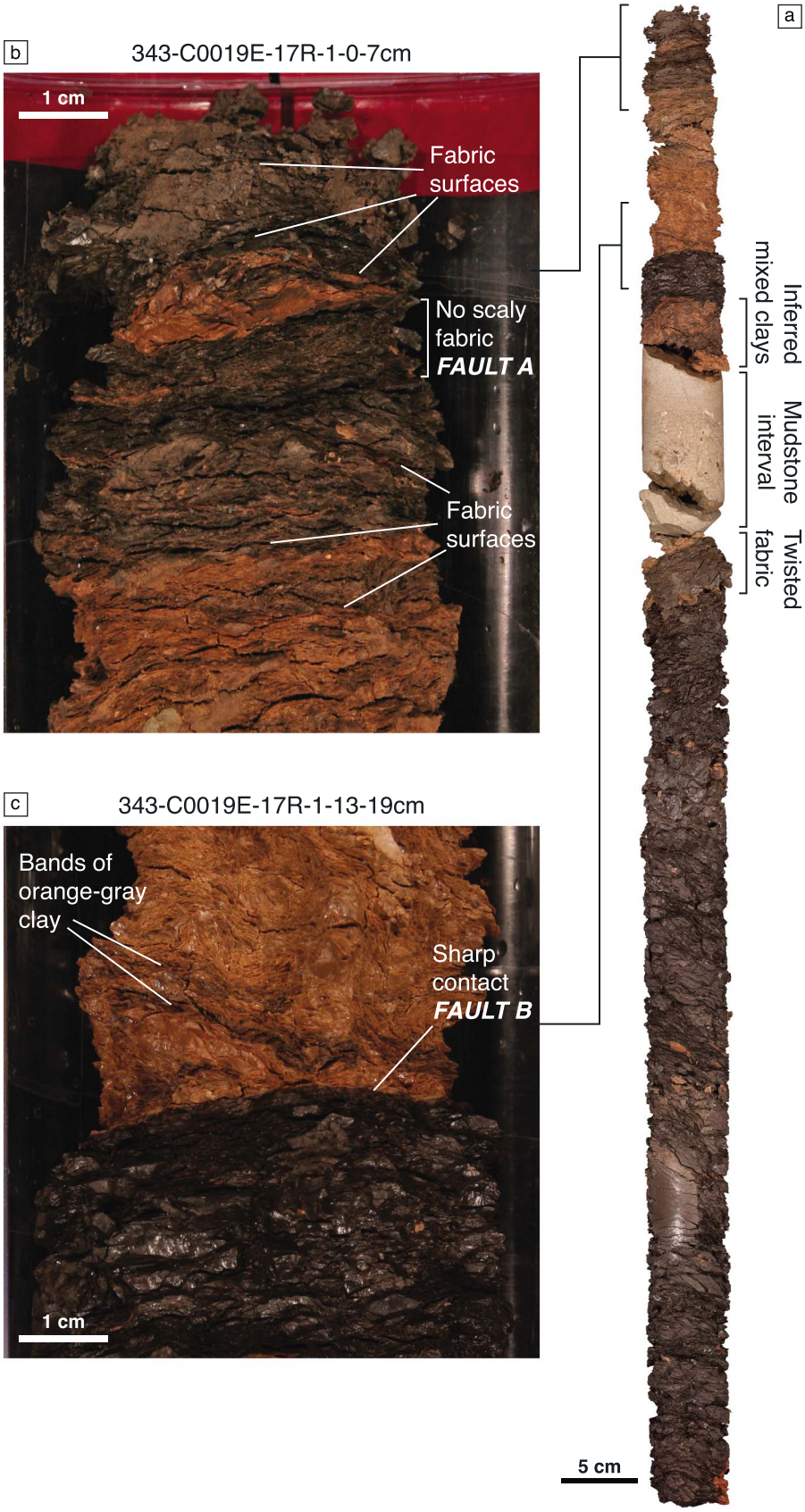

Figure 5

the décollement reflector in seismic surveys [*Chester et al.*, 2013a, 2013b]. The orientation and magnitude of the anisotropy of magnetic susceptibility indicates horizontal shortening above 821.5 mbsf and vertical, uniaxial strain below [*Yang et al.*, 2013]. These observations are consistent with the overall architecture of the margin described above; the frontal prism is structurally complex, with moderately to steeply dipping units uptilted during horizontal shortening, whereas the down-going plate is characterized by shallowly dipping strata affected mostly by vertical compaction.

The lithologic contrast between the frontal prism and the Pacific Plate units is defined by prominent differences in the composition and ages of the rocks (Figure 3). Dark gray siliceous mudstones of the frontal prism (in cores 16R and above) overlie tan-brown hemipelagic mudstones of the incoming plate (cores 18R and below), and the grain size distribution of the Pacific Plate units shows a higher proportion of clay-sized grains. In addition, biostratigraphic ages show that the rocks immediately above the plate boundary are Pleistocene and the units below the plate boundary are Miocene [*Chester et al.*, 2013a].

The décollement coincides with a unit of pervasively deformed smectite-rich, "scaly" clay recovered in core 17R (see below). It contrasts strongly with mudstones in the prism above, which are fractured and faulted, but within which the primary bedding is not disrupted and the deformation not pervasive. Bedding and other primary sedimentary features are apparent below the scaly clay layer at approximately 824 mbsf, delimiting the upper contact of the Pacific Plate units. We therefore interpret the plate boundary to be localized within the scaly clay layer in the interval between the clearly defined frontal prism and Pacific Plate units [*c.f.*, *Chester et al.*, 2013b].

Core recovery was incomplete in the interval between the base of the frontal prism (~820 mbsf) and top of the Pacific Plate (~824 mbsf), but drilling logs show that the maximum drill bit advance in this interval was 4. m (Figure 3). As a first approximation, this interval represents the plate boundary fault zone [*Chester et al.*, 2013b]. However, subsidiary faults were observed in both the hanging wall and foot wall (see sections 3.1 and 3.2; Figure 3). Such structures define a broader fault zone around 7 m wide, which may have accommodated some of the total displacement across the plate boundary. The stratigraphy of the Pacific Plate units also suggests additional complexity in the footwall: the tan-brown Miocene mudstones directly overlie Cretaceous laminar pelagic clays at ~834 mbsf [*Chester et al.*, 2013a]. The incoming section described at DSDP Site 436 [*Arthur and Adelseck*, 1980] includes Early Miocene, Oligocene, and Eocene clays (Unit 3A) between the Miocene Unit 2 and Cretaceous Unit 3, suggesting that Unit 3A is missing at the JFAST site. The contact between the tan-brown mudstone and Cretaceous pelagic clay (Figure 4b) is therefore either a tectonic contact or a disconformity. If it is a tectonic contact, the maximum width of the plate boundary fault is around 15 m (Figure 3). This estimate is notably less than the ~50 m thick fractured and brecciated zone that defines the plate boundary thrust at the Nankai margin [*Ujiie and Kimura*, 2014], which is more typical for shallow subduction thrusts [*Rowe et al.*, 2013].

4.2. Composition of the Décollement

One core (core 17R) was recovered from within the décollement (Figure 5). Core 17R is composed predominantly of clay, with one short interval of more competent mudstone. The clay displays two colors: bright reddish orange-brown and dark chestnut brown to almost black. Radiolarian microfossils are absent in the clay in core 17R so the age has not been precisely determined. Pelagic clay at DSDP Site 436 is Early Miocene to Eocene [*Doyle and Riedel*, 1980]. The pelagic clay in the Pacific Plate at the JFAST site (core 21R) is Cretaceous (see section 3.2). Although the ages of these two units are different, they may be conformable units within the same sequence so either could correlate with the clay in core 17R, as noted by *Moore et al.* [2015]. The radiolarian microfossil assemblage in the short mudstone interval shows that it is the same age as the footwall units (Late Miocene).

Contacts separating the two colors in the clay are predominantly discrete, but locally, mixing between them is inferred (Figure 5). Immediately after removal from the core liner, both types of clay were extremely soft

Figure 5. (a) Photomontage of core 17R showing an image of the recovered whole round section recovered from the plate boundary décollement (photos viewed down onto top of working half; image courtesy JAMSTEC/IODP). (b) Zoomed-in photograph showing the interval where the scaly fabric is obliterated, providing evidence for localized deformation. (c) Zoomed-in photograph of the sharp contact located ~16 cm from the top of core 17R. Note that the bands of orange-gray clay and the scaly fabric are truncated against the contact.

Figure 6. Photograph of part of core 17R showing the polished surfaces that define the scaly fabric (white lines) and phacoids of clay (within white lines). Phacoid long axes (red lines) are aligned and shallowly plunging. Evidence for shear across the fabric surfaces (discussed in section 4.3) suggests they may be comparable to Y and P Riedel shears [*Rutter et al.*, 1986], which is shown schematically at the top of the figure (grey shape represents a single phacoid). The phacoid asymmetry and shear orientations are consistent with overthrusting. White arrows show examples of places where the contacts between dark brown and orange-brown clays are not co-located with the polished surfaces. Inset shows the polished face of a phacoid with lineations oriented up-down in this field of view.

and malleable. The top 22 cm of core 17R above the mudstone interval contains bands ~2–25 mm wide of alternating colors with variable luster. Orange-brown clay is predominant in this interval. The lower section of the core below the mudstone interval (35–100 cm) is predominantly shiny and dark brown with only subtle variations in color but contains some centimeter-scale, irregular bands of matte luster clay. Bright orange patches are locally abundant throughout the dark brown clay. Compositional differences between the two colors of clay are likely due to higher Fe or Mn oxides in the dark brown clay, but both clays are dominated by smectite [*Kameda et al.*, 2015; A. M. Schleicher et al., submitted manuscript, 2014]. Where the clay is predominantly dark brown, orange-brown patches are typically less than 1 cm long and have irregular shapes. Occasionally, the patches approximate asymmetric ellipses but are more frequently completely irregular. Smaller, millimeter-scale patches tend to be equant blocks. Generally, the boundaries between the two clay colors are sharp and do not coincide with surfaces that define the pervasive scaly fabric described below. This indicates that the boundaries overprint the scaly fabric, so the color difference is possibly an alteration or diagenetic effect. However, the millimeter-sized orange-brown patches with blocky shapes appear to be fragments that have been deformed, suggesting that the color-changing alteration both predates and postdates the scaly fabric.

The mudstone interval within core 17R is located ~23–35 cm below the top of the core (Figure 5a). This mudstone is pale grayish brown and is composed of ~40% silt and ~60% clay. Sugary, white patches several millimeters in diameter are likely volcaniclastic fragments. Numerous deformation bands and dark seams are present in at least two sets within the mudstone, with structures spaced every few centimeters. X-ray computed tomography measurements indicate that the deformation bands have higher density than the surrounding mudstone, suggesting that their formation caused a reduction in porosity through compaction and therefore that they may be compaction bands [*Fossen et al.*, 2007]. Two dominant orientations of structures were identified: one dipping ~25–35° and another dipping ~45–65°. The more shallowly dipping set crosscuts and offsets the more steeply dipping set. The boundaries between the scaly clay and the mudstone interval are deformed in a spiral fashion over a 2–3 cm interval within the clay, as if the clay was twisted during relative rotation associated

with core recovery (Figure 5a). As the twisted fabric overprints the tectonic fabrics, we infer that the primary characteristics of the contacts were overprinted by drilling disturbance.

4.3. Scaly Fabric

The recovered décollement clay contains a pervasive, spaced, anastomosing cleavage (Figure 6). This cleavage is geometrically similar to scaly fabrics observed at other subduction margins where they are associated with faults and stratigraphic inversions [e.g., *Lundberg and Moore*, 1986; *Moore et al.*, 1986; *Agar et al.*, 1989; *Prior and Behrmann*, 1990; *Labaume et al.*, 1997; *Vannucchi et al.*, 2003]. At Site C0019, the scaly fabric is defined by polished surfaces that display lineations (Figure 6). Lineations are predominantly grooves and ridges in the shapes of the surfaces rather than striations or tool marks. Tool marks are defined by *Doblas* [1998] as crescent markings, chatter marks, scour marks, gouge grooves and ridges, scratches, and striations that are examples of linear features produced by the wearing action of a hard indenter onto the opposing fault surface. The grooves and ridges we observe on the anastomosing surfaces are anisotropies on the polished surface shape (analogous to the fault surface roughness developed at meter scale observed, for example, by *Sagy et al.* [2007]).

Between the fabric surfaces, millimeters-long to centimeters-long, lenticular chips of clay with polished faces, herein termed phacoids, are completely nested. Phacoids have concave or convex faces separated by sharp corners. Lineations are parallel on any given face. The phacoids vary in size and shape, both locally and in general trends throughout the length of the core. In the upper section of the core (0–22 cm), phacoids are small (~1–7 mm in long axis), the long axes are very strongly aligned, and aspect ratios are low. In the lower section of the core (35–100 cm), the phacoids are generally larger (~3–15 mm long) and have a higher aspect ratio (Figure 6). No veins are observed within the interval of scaly clay.

The relatively homogeneous composition of the clay in core 17R means there are no bedding planes or other stratigraphic markers visible to indicate the amount of offset that might have developed across the scaly fabric surfaces. Boundaries between the dark brown and orange-brown clays described above do not coincide with phacoid boundaries and are not offset across the surfaces. However, the polished phacoid faces with lineations are consistent with shear displacement, and the phacoids have a shape asymmetry that indicates a component of simple shear [*Labaume et al.*, 1997; *Wojtal*, 2001], which may be used to infer the shear sense. The surfaces that separate the phacoids have two consistent dip magnitudes in the core reference frame, one of which is very shallow and one that is moderately steeper, both dipping in the plunge direction of the phacoid long axes (Figure 6). The shallowly dipping surfaces are subparallel to the décollement dip and the dips of the discrete faults described below and are therefore inferred to be subparallel to the décollement shear plane. Assuming that these two fabric orientations represent shear surfaces (compare with *Moore and Wheeler* [1978], *Moore et al.* [1986], and *Labaume et al.* [1997]), shallowly dipping, shear plane-parallel surfaces are geometrically analogous to Y and more steeply dipping surfaces to P shears [*Rutter et al.*, 1986]. Additional shear surfaces that could correspond to the R-orientation are not observed in the core face. Following paleomagnetic geographic reorientation of the core, the phacoid asymmetry indicates top-to-the-east simple shear, corresponding to the sense of shear in the subduction zone [*Mishima et al.*, 2013].

4.4. Discrete Faults Within the Décollement

Four faults are inferred or observed within core 17R. The lithologic and stratigraphic differences between the smectite-rich clay (Paleogene or older) and mudstone interval (Middle Miocene) suggest that the contacts at the upper and lower boundaries of the mudstone are tectonic, although as discussed above, these contacts are obscured by drilling disturbance. The mudstone interval therefore likely represents a tectonic sliver, or horse, of repeated material from the footwall (Figure 3).

Two additional faults show evidence of localized deformation within the clay (Figure 5). The upper fault, referred to here as Fault A, is located ~3–4 cm from the top of core 17R. Fault A is defined as a ~1 cm thick zone where the spaced cleavage is obliterated (Figure 5b). Within this zone, the clay is composed of equant, ≤1 mm long, angular blocks with no preferred orientation. Most blocks are dark brown, but some are orange-brown clay. Notably, the edges of blocks correspond to the contacts between different colors of clay. The upper edge of Fault A is sharp and juxtaposes the two-color foliated clay from the blocky clay, suggesting that the blocky zone crosscuts the scaly fabric. Down-section, the blocks within Fault A gradually coarsen over an interval of around 0.5 cm to a zone of intense scaly fabric containing 3–5 mm phacoids. The color of the intensely foliated clay in this interval is intermediate between the dark and orange browns,

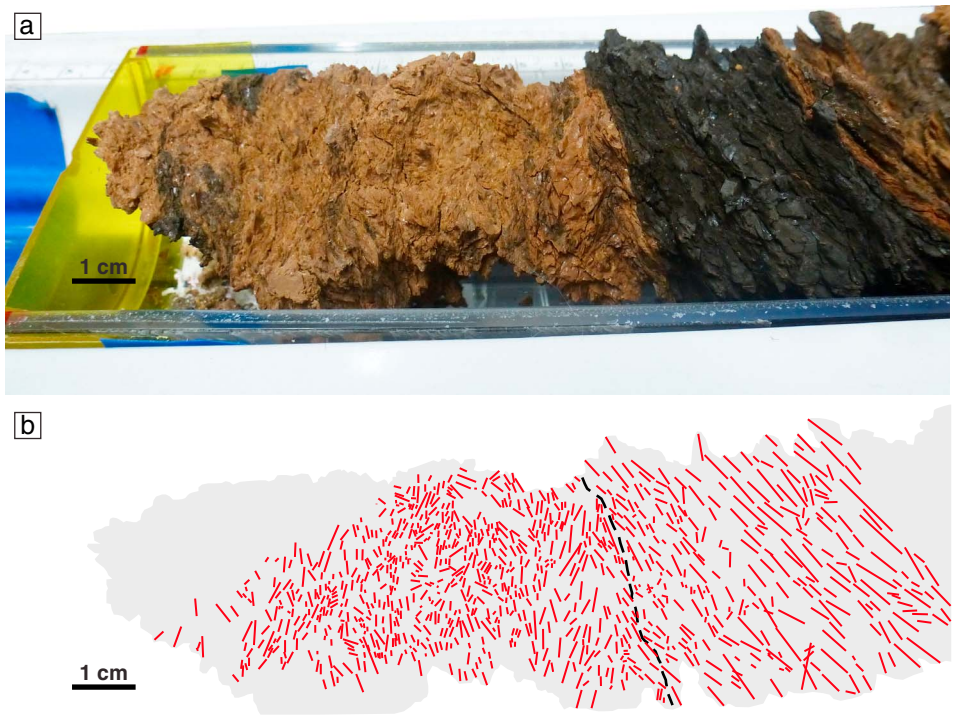

Figure 7. (a) Photograph of the upper section of core 17R showing the sharp contact between orange-brown (up-section on the left) and dark brown (down-section, right) clays that defines Fault B. (b) Sketch showing the orientations and lengths of phacoid long axes (red lines, similar to Figure 6). Although this is an oblique view of the core, the change in orientation and length of the phacoids is clear and is not a function of the orientation of the photo. Up-section, the phacoids are smaller and vary in orientation.

suggesting mixing of the two. In places, orange clay is present in extremely elongate, cleavage-parallel patches. The mixed zone is around 1.5 cm thick, below which the clay is predominantly orange.

Fault B is defined by a sharp contact between the orange-brown and dark brown clays at ~16 cm below the top of core 17R (Figures 5c and 7). This is the only place in the core where a contact between orange and dark brown clays spans the entire core diameter. The sharp contact is slightly wavy, with millimeter-scale amplitude undulations, but is not visibly defined by a layer of different material; the two colors of clay are juxtaposed sharply across the contact. Clay above Fault B is predominantly orange-brown, but contains several bands of darker, orange-gray clay. The bands are a few millimeters thick and are locally parallel to the orientation of the phacoid long axes. The dark brown clay below the fault is homogeneous, with only occasional millimeter-sized, isolated spots of orange-brown clay. Phacoids are smaller up-section of the contact in the orange-brown clay (~1–3 mm) and larger down-section in the dark brown clay (~3–10 mm). The scaly fabric in the dark brown and orange-brown clays is differently oriented on either side of the contact. Both the scaly fabric and bands of orange-gray clay are continuous up to Fault B and are truncated against it.

The microscopic structure of Fault B is more heterogeneous than is apparent from core observations. The contact consists of three submillimeter-thick layers (Figure 8). Each layer has sharp boundaries that are parallel to the overall orientation of the fault, which is subparallel to the Y-foliation orientation discussed in section 4.3. The long axes of aligned clay grains (typically a few micrometers long) define a microscopic foliation inside the layers. Near the boundaries between the layers, this foliation is deflected slightly to form a sigmoidal geometry consistent with the inferred sense of shear across the scaly fabric (see Figure 8). The upper and lower edges of Fault B are slightly wavy and truncate the fabric on either side. Structurally above the fault, the orange-brown clay contains phacoids of variable size and shape chaotically arranged in a matrix with a weak fabric defined by aligned clay grains. Below the fault, the dark brown clay contains aligned phacoids 1–5 mm long. In both colors of clay, bands ≤100 μm thick of aligned grains define the edges of the phacoids.

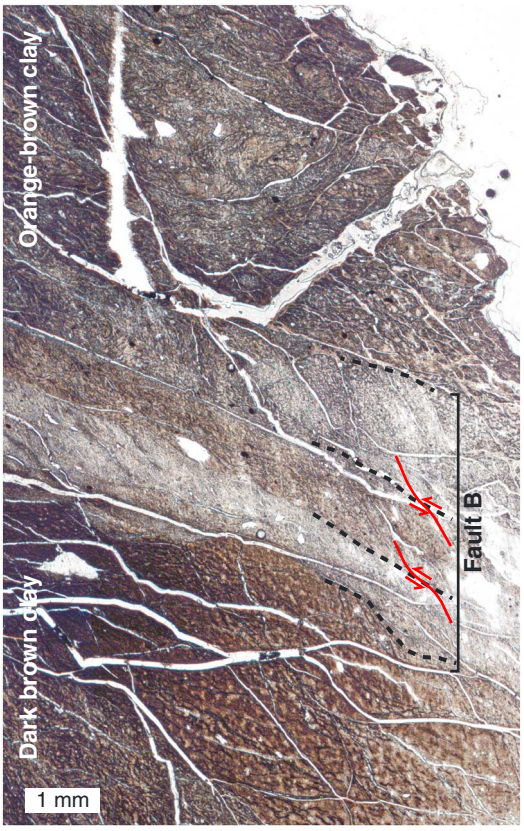

Figure 8. Photomicrograph (plane-polarized light) of Fault B in core 17R. The fault contains three layers, the boundaries of which are indicated by the dashed black lines. Aligned long axes of clay grains define a microscopic foliation within the layers (note that individual clay grains are too small to see at this scale of observation). Near the layer boundaries, the microscopic foliation has a sigmoidal shape, shown by red lines.

5. Discussion

The observations presented above document the transition from frontal prism units to Pacific Plate-affinity sedimentary units at around 821 mbsf. The transition coincides with the most deformed rock encountered in the core at the JFAST study site. Below, we discuss the overall geometry of the plate boundary and the possible processes by which fault rock textures within the décollement formed.

5.1. Structure of the Plate Boundary Fault Zone

The plate boundary contains multiple faults with a complex overall structure. The precise geometry is not well constrained due to the incomplete recovery and lack of displaced markers in the cores that could have been used to establish shear sense and displacement. One possible model is shown in Figure 9, which includes the locations of faults observed in the core and also those that are inferred from biostratigraphic age reversals and/or gaps. In this model, all of the faults are reverse, which is assumed where there are no direct observational constraints. Most of the thrusts are oriented subparallel to the décollement, with a few more steeply dipping structures in between.

In this geometry, the faults define a duplex structure with the roof thrust at the base of the frontal prism and the sole within or below the Pacific Plate Miocene mudstones. The most significant fault contacts occur at the top and base of core 17R bounding the layer of smectite-rich, scaly clay (Figure 3). The lack of microfossils

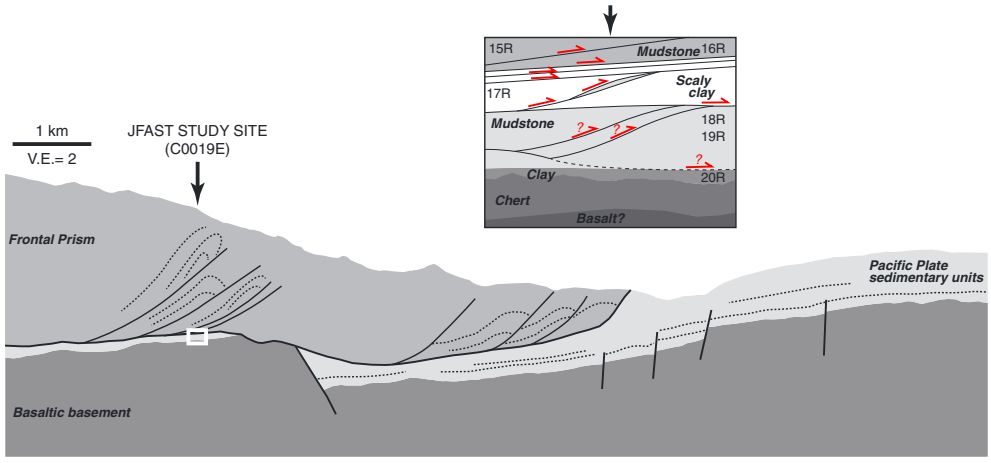

Figure 9. Schematic representation of the structures observed within the plate boundary zone at the JFAST study site. Main image shows a simplified interpretation of the seismic reflection images (see Figure 1). Faults (solid lines) and bedding orientations (dotted lines) are shown schematically. Inset shows the internal structure of the plate boundary zone and corresponds to the white box at the décollement below the JFAST study site location. Faults are shown as black lines, lithologic contacts as changes in lithology (color) without black lines. The dashed fault corresponds to the base of the Miocene mudstone section below core 17R (see section 5.1 for discussion).

in the smectite-rich clay in core 17R means the age of the clay is currently poorly constrained. It could be stratigraphically equivalent to either the pelagic clay near the base of the cored interval (core 20R) or the Neogene pelagic clay at Site 436 [*Moore et al.*, 2015]. In either case, there must be an age gap at the base of the frontal prism, and a significant age reversal at the base of core 17R. This implies that the geometry shown in Figure 9 is specific to the JFAST site: the presence of the pelagic clay structurally above the Miocene mudstone is a repetition of stratigraphy that suggests the sole thrust must be located within the pelagic clay elsewhere, presumably landward of the JFAST site.

The significance of the structurally lowest contact in core 20R between the Miocene mudstone and the Cretaceous pelagic clay is ambiguous (shown in Figure 4b and dashed in Figure 9). Although the bedding attitude measurements show a slight change in dip across the contact, there is no evidence that the pinkish layer at the base of the mudstone contains fault rock, and there is very little deformation in the mudstone or the clay (which notably does not have a scaly fabric; Figure 4b). This suggests that the contact is not tectonic. However, there is a significant age gap between the two units. Disconformities were not reported in the reference section at Site 436 [*Arthur and Adelseck*, 1980], so the stratigraphic constraints indicate complexity that could be explained by a faulted contact.

Faults with apparent normal offsets and a large number of steeply dipping subsidiary structures identified in the JFAST core [*Chester et al.*, 2013a] suggest that the model shown in Figure 9 could be oversimplified. Combined with the normal faults observed cutting the input section in the seismic survey images (Figure 2) and normal faults observed within the décollement at other margins (e.g., Barbados; *Shipley et al.* [1995]), the data suggest that some of the faults in Figure 9 may be normal rather than reverse, particularly in the lower plate where vertical compaction is inferred from magnetic susceptibility data [*Yang et al.*, 2013]. However, the majority of the observations support shortening and imbrication of the décollement and structurally lower section. The JFAST study site was located above a horst in the down-going plate where seismic images show a thin packet of subducted sediments below the décollement reflector and above the top of the basaltic basement. The sediment packet is approximately 75 m thick, which is considerably thinner than the corresponding stratigraphy on the incoming plate (see Figure 2). This suggests that much of the incoming section was off-scraped and should be present in the frontal prism, consistent with the predominant Pleistocene age of many of the hemipelagic mudstones in the frontal prism. Bedding attitudes and fault orientations in the prism define a fold-and-thrust geometry [*Chester et al.*, 2013a]. Repetition of the pelagic clay in the plate boundary zone implies that the décollement is a zone of imbrication where meter-thick to 10 m thick units are intercalated (Figure 9).

Despite the uncertainties outlined above, the model shown in Figure 9 is consistent with the overall architecture of the margin. Interpretation of seismic reflection images has shown that the accretion of pelagic and hemipelagic sediments to the wedge is episodic and complicated by the subduction of basement horsts and grabens, and some degree of frontal reworking is likely [*Nakamura et al.*, 2013]. Our observation of multiple faults within the subducting section between ~821 and 831 mbsf, subparallel to stratigraphy, implies that the down-going sedimentary section has been sliced at a low angle to the décollement. These faults may have accommodated some of the plate motion but, as they are roughly parallel to stratigraphy, do little to explain the missing strata between the Cretaceous and Miocene clays.

5.2. Deformation in the Décollement

Structures resulting from two distinct styles of deformation are present in the fault rocks recovered from within the plate boundary zone: the scaly fabric which is distributed throughout the smectite-rich clay in core 17R and the sharp, localized faults observed or inferred at several places in the core.

The scaly fabric is present throughout the clay in core 17R, and we infer that it formed from an increment of strain which was distributed across the clay interval. This deformation is defined by one set of fabric surfaces oriented subparallel to the overall décollement orientation observed in seismic surveys [e.g., *Nakamura et al.*, 2013] as well as another more steeply dipping set. Lineations and the luster of the fabric surfaces indicate grain alignment and relative displacement across phacoid boundaries, suggesting that the fabric surfaces correspond to Y and P shears [*Rutter et al.*, 1986] distributed across a meter-scale shear zone. The scaly fabric varies in intensity within the core. Intensity here refers to the spacing of the polished surfaces and size of the phacoids between them that define the fabric. Near the top of core 17R, the surfaces are closely spaced, with millimeter-scale phacoids (e.g., Figure 7). The phacoid size and surface spacing increases gradually down-core to centimeter scale in the lower half (Figure 5a). As there is no evidence for a material

change within the clay near the top of the core, the change in size of the phacoids could indicate a spatial variation in the finite strain within the material. This variation in the intensity of deformation could not be explained by compaction or diagenesis, as these would have affected the whole clay section in core 17R equally.

Faults cut the scaly fabric in at least four places within core 17R showing that localized brittle deformation also occurred at multiple stages in the deformation history. Faults A and B described in section 4.4 are subparallel both to the overall dip of the décollement and to the Y shears in the scaly fabric. The sigmoidal geometry of the microscopic foliation within Fault B is also consistent with thrust-related deformation within the décollement (Figure 8), suggesting that the sharp contacts are kinematically compatible with the scaly fabric. However, Faults A and B clearly locally crosscut the scaly fabric, juxtaposing slightly differently oriented fabric domains in the case of Fault B, indicating that these two types of structures form independently. A similar inference can be made for the faults bounding the mudstone interval in core 17R, which must have cut up-section to repeat the clay above the mudstone.

The formation of both distributed and localized structures at different times within the décollement is consistent with the frictional properties of smectite-rich fault rocks. Rock friction experiments show that smectite-rich materials are predominantly velocity-neutral or velocity-strengthening at low velocities [*Saffer and Marone*, 2003; *Ikari et al.*, 2007; *Faulkner et al.*, 2011; *Ferri et al.*, 2011; *Sawai et al.*, 2014; *Ikari et al.*, 2015] and velocity-weakening at high velocities [*Ferri et al.*, 2011; *Faulkner et al.*, 2011; *Ujiie et al.*, 2013; *Sawai et al.*, 2014; *French et al.*, 2014], with both characteristics promoted by water saturation. Distributed shearing has been associated with velocity-strengthening behavior in friction experiments [e.g., *Beeler et al.*, 1996; *Logan et al.*, 1992; *Scruggs and Tullis*, 1998]. For example, *French et al.* [2014] describe results from rotary shear friction experiments on wet, smectite-rich materials that produce a strong foliation though the majority of the clay oriented at angles up to 30° to the shear zone boundaries, with a minor foliation parallel to the shear plane. Foliation planes are defined by color bands in thin section and are observed to coincide with unloading cracks formed after shearing. They are inferred to be precursory to displacement weakening [*French et al.*, 2014]. The geometric arrangement, microscopic appearance, and tendency to form parting surfaces of these foliation planes are similar to the scaly fabric in core 17R. If the scaly fabric in core 17R is correlative to this texture, it most likely represents a low strain rate, velocity-strengthening, displacement-strengthening texture. Low strain rates and/or strain-hardening behavior have been inferred to cause scaly fabric to form in other décollements due to pore pressure decrease, frictional strengthening, or rotation of the scaly fabric shear planes to suboptimal orientations [*Moore et al.*, 1986].

Localized slip that characterizes the faults in core 17R is predicted for velocity-weakening behavior [e.g., *Rice*, 2006] and is observed in experiments conducted at seismic slip rates [*Ujiie et al.*, 2013; *French et al.*, 2014]. No direct evidence for high strain rates has been reported from the JFAST faults to date, but there are similarities between the experimental slip zones and Fault B (Figure 8): the fault is ~3 mm thick and is made up of submillimeter layers that contain a grain-scale foliation defined by the aligned long axes of clay grains (see section 4.4). Both the degree of localization and alignment of clay grains within a narrow layer are observed when smectite-rich clays are sheared at seismic slip rates under saturated, undrained conditions but not when the slip rate is less than tens of centimeters per second [*Ujiie et al.*, 2013; *French et al.*, 2014]. By analogy with the experimental results, these similarities suggest that the discrete fault may have formed in saturated clay at seismic slip rates, coeval with weakening by thermal pressurization.

We therefore suggest that the scaly fabric and the discrete faults formed respectively by distributed (aseismic) and localized (seismic) slip in the décollement. Elevated strain rates can only have been achieved during earthquake slip in the shallow part of the subduction zone, and as the faults are décollement-parallel, it is possible that the discrete faults cutting the clay represent paleoseismic rupture surfaces. There have been no ocean-bottom GPS deployments near the JFAST study site to monitor for recent creep at the toe of the wedge, but the distributed fabrics described here suggest that creep on the plate boundary fault occurred in between earthquakes in the past. We infer that the rheology of the pelagic clay involves both velocity-strengthening or velocity-neutral, strain-hardening behavior at low strain rate and velocity-weakening behavior at high strain rates. This indicates that the shallow portion of the Japan Trench may be better characterized as conditionally stable rather than stable [*Scholz*, 1998]. Additionally, our

observations provide geologic support for velocity-dependent stability of smectite-rich clays [*Sawai et al.*, 2014; *Ikari et al.*, 2015].

Scaly fabrics similar to those described here have been reported in faults from several other margins including the northern Barbados Ridge, Marianas trench, southern Mexico, and Guatemala [*Lundberg and Moore*, 1986; *Labaume et al.*, 1997]. Scaly fabrics are common in the décollement of the northern Bardados ridge [e.g., *Behrmann et al.*, 1988; *Shipley et al.*, 1995; *Labaume et al.*, 1997], where the deformed clay also contains discrete surfaces across which the fabric orientation changes [*Labaume et al.*, 1997]. The geometry of those structures is similar to that reported here. Further work is required to verify the seismic origin of the localized slip zones in the JFAST core, and the structures that may be present in the sections of the fault zone that were not recovered remain unknown. As earthquake nucleation close to the trench is unlikely given the frictional properties of the fault zone clay [*Faulkner et al.*, 2011; *Sawai et al.*, 2014; *Ikari et al.*, 2015], the observation that multiple slip surfaces are present within core recovered from the plate boundary zone indicates that fault slip at shallow depth may have occurred repeatedly since the footwall was first subducted at this site. Rupture to the trench may therefore be a characteristic behavior of the Japan Trench and other margins that contain similar deformation structures.

6. Conclusions

Core recovered from in and around the décollement at the JFAST study site shows that the frontal prism near the trench is composed of moderately to steeply dipping, off-scraped Miocene and younger hemipelagic mudstones. Subducted Pacific Plate units are comparatively more clay-rich Miocene mudstones and Cretaceous clay and chert with low bedding dips. The interval between the frontal prism and Pacific Plate defines the plate boundary, which is localized onto $\leq$4.86 m of smectite-rich, scaly clay, of which $\sim$1 m was recovered. Faults surrounding the scaly clay delimit a zone 5 to 15 m wide in which faults parallel to bedding may have accommodated some plate motion. The scaly fabric is interpreted to have formed at low strain rates, likely in response to deformation at close to plate motion rates. This is consistent with the velocity-strengthening frictional stability often observed experimentally for smectite-rich clays. Multiple discrete shear surfaces cut the clay. Evidence for extreme slip localization and clay alignment within the slip zones suggests that these structures formed at high strain rates, likely driven by seismic slip. The clay at the Japan Trench therefore exhibits evidence for both low strain rate, strain-hardening and/or velocity-strengthening behavior and high strain rate, velocity-weakening behavior. The structures documented here indicate that slip to the trench has occurred repeatedly at the JFAST site and may be expected at other margins where the frontal thrust is localized onto pelagic clay.

Acknowledgments
This research used samples and data provided by the Integrated Ocean Drilling Program (IODP). Images and core description logs used in this study are available for download from IODP. We thank the science party of Expedition 343/343T for their dedication to the project and insightful discussions during and since the expedition. This work was only possible thanks to the historic engineering accomplishments of the drilling, logging, and operational team of D/V *Chikyu*. Thanks to Tucker Keren for reviewing an early version of this manuscript. Thanks to Susan Cashman for a thorough and thoughtful review. Kirkpatrick was supported by a U.S. Science Support Program Post-Expedition award and NSF award OD 1260602.

References

Agar, S. M., D. J. Prior, and J. H. Behrmann (1989), Back-scattered electron imagery of the tectonic fabrics of some fine-grained sediments: Implications for fabric nomenclature and deformation processes, *Geology*, *17*(10), 901–904.

Argus, D. F., R. G. Gordon, and C. DeMets (2011), Geologically current motion of 56 plates relative to the no-net-rotation reference frame, *Geochem. Geophys. Geosyst.*, *12*, Q11001, doi:10.1029/2011GC003751.

Arthur, M. A., and C. G. Adelseck Jr. (1980), Acknowledgments, introduction, and explanatory notes: The Japan trench transect, Legs 56 and 57, Deep Sea Drilling Project, in *Initial Reports of the Deep Sea Drilling Project*, vol. 56–57, edited by M. Lee and L. N. Stout, pp. 3–21, doi:10.2973/dsdp.proc.5657.1980.

Beeler, N. M., T. E. Tullis, M. L. Blanpied, and J. D. Weeks (1996), Frictional behavior of large displacement experimental faults, *J. Geophys. Res.*, *101*(B4), 8697–8715.

Behrmann, J. H., et al. (1988), Evolution of structures and fabrics in the Barbados accretionary prism. Insights from leg 110 of the Ocean Drilling Program, *J. Struct. Geol.*, *10*(6), 577–591.

Carson, B., R. von Huene, and M. Arthur (1982), Small-scale deformation structures and physical properties related to convergence in Japan Trench slope sediments, *Tectonics*, *1*(3), 277–302.

Chester, F. M., J. Mori, N. Eguchi, S. Toczko, and the Expedition 343/343T Scientists (2013a), Japan Trench Fast Earthquake Drilling Project (JFAST), in *Proceedings of the IODP*, vol. 343/343T, Integrated Ocean Drilling Program Management International, Inc., College Station, Tex., doi:10.2204/iodp.proc.343343T.2013.

Chester, F. M., et al. (2013b), Structure and composition of the plate-boundary slip-zone for the 2011 Tohoku-oki earthquake, *Science*, *342*, 1208–1211.

DeMets, C., R. G. Gordon, and D. F. Argus (2010), Geologically current plate motions, *Geophys. J. Int.*, *181*, 1–80.

Doblas, M. (1998), Slickenside kinematic indicators, *Tectonophysics*, *295*, 187–197.

Doyle, P. S., and W. R. Riedel (1980), Ichthyoliths from site 436, northwest Pacific, leg 56, deep sea drilling project, in *Initial Reports of the Deep Sea Drilling Project 56–57 Part 2*, vol. 56, pp. 887–893, Texas A & M University, Ocean Drilling Program, College Station, Tex., doi:10.2973/dsdp.proc.5657.127.1980.

Faulkner, D. R., T. M. Mitchell, J. Behnsen, T. Hirose, and T. Shimamoto (2011), Stuck in the mud? Earthquake nucleation and propagation through accretionary forearms, *Geophys. Res. Lett.*, *38*, L18303, doi:10.1029/2011GL048552.

Ferri, F., G. Di Toro, T. Hirose, R. Han, H. Noda, T. Shimamoto, M. Quaresimin, and N. de Rossi (2011), Low-to high-velocity frictional properties of the clay-rich gouges from the slipping zone of the 1963 Vaiont Slide, northern Italy, *J. Geophys. Res.*, *116*, B09208, doi:10.1029/2011JB008338.

Fossen, H., R. A. Schultz, Z. K. Shipton, and K. Mair (2007), Deformation bands in sandstone: A review, *J. Geol. Soc. London*, *164*(4), 755–769.

French, M. E., H. Kitajima, J. S. Chester, F. M. Chester, and T. Hirose (2014), Displacement and dynamic weakening processes in smectite-rich gouge from the central deforming zone of the San Andreas Fault, *J. Geophys. Res. Solid Earth*, *119*, 1777–1802, doi:10.1002/2013JB010757.

Fujii, Y., K. Satake, S. Sakai, M. Shinohara, and T. Kanazawa (2011), Tsunami source of the 2011 off the Pacific coast of Tohoku earthquake, *Earth Planets Space*, *63*, 815–820.

Fujiwara, T., S. Kodaira, T. No, Y. Kaiho, N. Takahashi, and Y. Kaneda (2011), The 2011 Tohoku-oki earthquake: Displacement reaching the trench axis, *Science*, *334*(6060), 1240–1240, doi:10.1126/science.1211554.

Fulton, P., et al. (2013), Low coseismic friction on the Tohoku Fault determined from temperature measurements, *Science*, *342*(6163), 1214–1217.

Hasegawa, A., K. Yoshida, Y. Asano, T. Okada, T. Iinuma, and Y. Ito (2012), Change in stress field after the 2011 great Tohoku-Oki earthquake, *Earth Planet. Sci. Lett.*, *355-356*, 231–243.

Hashimoto, C., A. Noda, T. Sagiya, and M. Matsu'ura (2009), Interpolate seismogenic zones along the Kuril-Japan trench inferred from GPS data inversion, *Nat. Geosci.*, *2*, 141–144.

Ide, S., A. Baltay, and G. C. Beroza (2011), Shallow dynamic overshoot and energetic deep rupture in the 2011 M_w 9.0 Tohoku-oki earthquake, *Science*, *332*, 1426–1429.

Ikari, M. J., D. M. Saffer, and C. Marone (2007), Effect of hydration state on the frictional properties of montmorillonite-based fault gouge, *J. Geophys. Res.*, *112*, B06423, doi:10.1029/2006JB004748.

Ikari, M. J., C. Marone, and D. M. Saffer (2011), On the relation between fault strength and frictional stability, *Geology*, *39*(1), 83–86, doi:10.1130/G31416.1.

Ikari, M. J., J. Kameda, D. M. Saffer, and A. J. Kopf (2015), Strength characteristics of Japan Trench borehole samples in the high-slip region of the 2011 Tohoku-Oki earthquake, *Earth Planet. Sci. Lett.*, *412*, 35–41, doi:10.1016/j.epsl.2014.12.014.

Ito, Y., T. Tsuji, Y. Osada, M. Kido, D. Inazu, Y. Hayashi, H. Tsushima, R. Hino, and H. Fujimoto (2011), Frontal wedge deformation near the source region of the 2011 Tohoku-oki earthquake, *Geophys. Res. Lett.*, *38*, L00G05, doi:10.1029/2011GL048355.

Kameda, J., M. Shimizu, K. Ujiie, T. Hirose, M. Ikari, J. Mori, K. Oohashi, and G. Kimura (2015), Pelagic smectite as an important factor in tsunamigenic slip along the Japan Trench, *Geology*, in press.

Kanamori, H., M. Miyazawa, and J. Mori (2006), Investigation of the earthquake sequence off Miyagi prefecture with historical seismograms, *Earth Planets Space*, *58*, 1533–1541.

Kodaira, S., T. No, Y. Nakamura, T. Fujiwara, Y. Kaiho, S. Miura, N. Takahashi, Y. Kaneda, and A. Taira (2012), Coseismic fault rupture at the trench axis during the 2011 Tohoku-oki earthquake, *Nat. Geosci.*, *5*, 646–650.

Labaume, P., A. J. Maltman, A. Bolton, D. Tessier, Y. Ogawa, and S. Takizawa (1997), 4. Scaly fabrics in the sheared clays from the decollement zone of the Barbados accretionary prism, in *Proceedings of the Ocean Drilling Program, Scientific Results*, vol. 156, edited by T. H. Shipley et al., pp. 59–77, Ocean Drilling Program, College Station, Tex.

Lay, T., C. J. Ammon, H. Kanamori, L. Xue, and M. J. Kim (2011), Possible large near-trench slip during the 2011 M_w 9.0 off the Pacific coast of Tohoku earthquake, *Earth Planets Space*, *63*, 687–692.

Lin, W., et al. (2013), Stress state in the largest displacement area of the 2011 Tohoku-oki earthquake, *Science*, *339*, 687–690.

Logan, J. M., C. A. Dengo, N. G. Higgs, and Z. Z. Wang (1992), Fabrics of experimental fault zones: Their development and relationship to mechanical behavior, in *Fault Mechanics and Transport Properties of Rocks, International Geophysics*, vol. 51, edited by B. Evans and T.-F. Wong, pp. 33–67, Academic Press. [Available at http://store.elsevier.com/Academic-Press/IMP_5/.]

Lundberg, N., and J. C. Moore (1986), Macroscopic structural features in deep sea drilling project cores from forearc regions, *Geol. Soc. Am. Mem.*, *166*, 13–44.

Marone, C. (1998), Laboratory-derived friction laws and their application to seismic faulting, *Annu. Rev. Earth Planet. Sci.*, *26*, 643–696.

Mishima, T., et al. (2013), Paleomagnetic records of core samples of the plate-boundary thrust drilled during the IODP Japan Trench Fast Drilling Project (JFAST), in AGU Fall Meeting Abstracts, vol. 1, p. 2603.

Moore, J. C., and R. L. Wheeler (1978), Structural fabric of a melange, Kodiak Islands, Alaska, *Am. J. Sci.*, *278*, 739–765.

Moore, J. C., S. Roeske, D. S. Cowan, N. Lundberg, E. Gonzales, J. Schoonmaker, and S. E. Lucas (1986), Scaly fabrics from Deep Sea Drilling Project cores from forearcs, *Geol. Soc. Am. Mem.*, *166*, 55–74.

Moore, J. C., T. Plank, F. M. Chester, P. Polissar, and H. Savage (2015), The plate boundary thrust of the 2011 great Tohoku earthquake: Oceanographic provenance and controls on slip propagation, *Geosphere*, in press.

Nakamura, Y., S. Kodaira, S. Miura, C. Regalla, and N. Takahashi (2013), High-resolution seismic imaging in the Japan Trench axis area off Miyagi, northeastern Japan, *Geophys. Res. Lett.*, *40*, 1713–1718, doi:10.1002/grl.50364.

Niemeijer, A., G. Di Toro, W. A. Griffith, A. Bistacchi, S. A. F. Smith, and S. Nielsen (2012), Inferring earthquake physics and chemistry using an integrated field and laboratory approach, *J. Struct. Geol.*, *39*, 2–36.

Pollitz, F. F., R. Bürgmann, and P. Banerjee (2011), Geodetic slip model of the 2011 *M*9.0 Tohoku earthquake, *Geophys. Res. Lett.*, *38*, L00G08, doi:10.1029/2011GL048632.

Prior, D. J., and J. H. Behrmann (1990), Thrust-related mudstone fabrics from the Barbados forearc: A backscattered scanning electron microscope study, *J. Geophys. Res.*, *95*(B6), 9055–9067.

Rice, J. R. (2006), Heating and weakening of faults during earthquake slip, *J. Geophys. Res.*, *111*, B05311, doi:10.1029/2005JB004006.

Rice, J. R., and M. Cocco (2007), Seismic fault rheology and earthquake dynamics, in *Tectonic Faults: Agents of Change on a Dynamic Earth*, pp. 99–137, The MIT Press, Cambridge, Mass.

Rowe, C. D., J. C. Moore, F. Remitti, and IODP Expedition 343/343T Science Party (2013), The thickness of subduction plate boundary faults from the seafloor into the seismogenic zone, *Geology*, *41*(9), 991–994.

Rutter, E., R. Maddock, S. Hall, and S. White (1986), Comparative microstructures of natural and experimentally produced clay-bearing fault gouges, *Pure Appl. Geophys.*, *124*(1–2), 3–30.

Saffer, D., and C. Marone (2003), Comparison of smectite- and illite-rich gouge frictional properties: Application to the updip limit of the seismogenic zone along subduction megathrusts, *Earth Planet. Sci. Lett.*, *6793*, 1–17.

Sagy, A., E. E. Brodsky, and G. Axen (2007), Evolution of fault-surface roughness with slip, *Geology*, *35*(3), 283–286.

Sawai, M., T. Hirose, and J. Kameda (2014), Frictional properties of incoming pelagic sediments at the Japan Trench: Implications for large slip at a shallow plate boundary during the 2011 Tohoku earthquake, *Earth Planets Space*, *66*(1), 65.

Scholz, C. H. (1998), Earthquakes and friction laws, *Nature*, *391*, 37–42.
Scruggs, V., and T. Tullis (1998), Correlation between velocity dependence of friction and strain localization in large displacement experiments on feldspar, muscovite and biotite gouge, *Tectonophysics*, *295*(1), 15–40.
Shipley, T., et al. (1995), Site 948, in *Proceedings of the Ocean Drilling Program, Initial Reports*, vol. 156, pp. 87–192, Ocean Drilling Program, College Station, Tex.
Tsuru, T., J.-O. Park, S. Miura, S. Kodaira, Y. Kido, and T. Hayashi (2002), Along-arc structural variation of the plate boundary at the Japan Trench margin: Implication of interplate coupling, *J. Geophys. Res.*, *107*(B12), 2357, doi:10.1029/2001JB001664.
Tsuru, T., S. Miura, J.-O. Park, A. Ito, G. Fujie, Y. Kaneda, T. No, T. Katayama, and J. Kasahara (2005), Variation of physical properties beneath a fault observed by a two-ship seismic survey off southwest Japan, *J. Geophys. Res.*, *110*, B05405, doi:10.1029/2004JB003036.
Ujiie, K., and G. Kimura (2014), Earthquake faulting in subduction zones: Insights from fault rocks in accretionary prisms, *Prog. Earth Planet. Sci.*, *1*(1), 1–30.
Ujiie, K., A. J. Maltman, and M. Sánchez-Gómez (2004), Origin of deformation bands in argillaceous sediments at the toe of the Nankai accretionary prism, southwest Japan, *J. Struct. Geol.*, *26*(2), 221–231, doi:10.1016/j.jsg.2003.06.001.
Ujiie, K., et al. (2013), Low coseismic shear stress on the Tohoku-Oki megathrust determined from laboratory experiments, *Science*, *342*, 1211–1214.
Vannucchi, P., A. Maltman, G. Bettelli, and B. Clennell (2003), On the nature of scaly fabric and scaly clay, *J. Struct. Geol.*, *25*, 673–688.
von Huene, R., M. Langseth, N. Nasu, and H. Okada (1982), A summary of Cenozoic tectonic history along the IPOD Japan Trench transect, *Geol. Soc. Am. Bull.*, *93*(9), 829–846.
Wojtal, S. F. (2001), The nature and origin of asymmetric arrays of shear surfaces in fault zones, *Geol. Soc. London Spec. Publ.*, *186*, 171–193.
Yang, T., T. Mishima, K. Ujiie, F. M. Chester, J. J. Mori, N. Eguchi, S. Toczko, and E. Scientists (2013), Strain decoupling across the décollement in the region of large slip during the 2011 Tohoku-oki earthquake from anisotropy of magnetic susceptibility, *Earth Planet. Sci. Lett.*, *381*, 31–38.
Yue, H., and T. Lay (2011), Inversion of high-rate (1 sps) GPS data for rupture processes of the 11 March 2011 Tohoku earthquake (M_w 9.1), *Geophys. Res. Lett.*, *38*, L00G09, doi:10.1029/2011GL048700.